SUPPRESSION OF FRACTURE FAILURE OF STRUCTURES BY COMPOSITE DESIGN BASED ON FRACTURE MECHANICS

Victor C. Li and Shuxin Wang
Department of Civil and Environmental Engineering
University of Michigan, USA

ABSTRACT

This paper discusses the use of fracture mechanics for the microstructure tailoring of a fiber reinforced Engineered Cementitious Composite (ECC) to achieve extreme tensile ductility at the composite scale. It demonstrates that fracture mechanics applied to control fracture phenomena at the micro and meso material scales can lead to suppression of fracture failure at the macro structural scale. Specifically, models of tunneling crack at the fiber/matrix interface and the steady state propagation of bridged flat matrix crack combine to provide insights on composite design. Interestingly, the micromechanics model indicates that low fiber/matrix interface fracture energy and low mortar matrix fracture energy are desirable for attaining high composite ductility. These concepts are verified by an expanding set of experimental data on structural elements tested to failure. The explicit suppression of commonly observed fracture mechanisms in reinforced concrete columns under reverse cyclic loading when the concrete is replaced by ECC is described.

1 INTRODUCTION

In the past, fracture of concrete has led to catastrophic failures of structures. The concrete pier footing fracture that led to the collapse of multiple spans of the Schoharie Creek Thruway Bridge in 1987 is a good example. More recently, a number of structures that collapsed during the 1994 Kobe earthquake revealed very clear brittle fracture patterns. Despite steel reinforcements, the innate brittle behavior of concrete subjects concrete structures vulnerable to severe loading.

Although often overlooked, the lack of durability of reinforced concrete structures is also closely linked to the brittle nature of concrete. Drying shrinkage of concrete structural elements have led to deterioration and premature reaching of the servicability limit states of these structures, resulting in expensive maintenance schedule and cost.

To reduce the likelihood of failure under ultimate limit states or servicability limit states, the fracture phenomenon in concrete must be intrinsically suppressed. This means that concrete material with significantly higher toughness, or better still, higher tensile ductility needs to be developed to meet these needs. Paradoxically, fiber reinforced concrete (FRC) which has higher toughness than normal concrete, has not experienced wide-spread use, while high strength concrete which has higher brittleness than normal concrete, has gained significant ground in practical applications in the last decade. While there are good reasons for this turn of events, it remains a fact that today our infrastructure may be even more severely prone to fracture failure under catastrophic events and unexpected premature deterioration during normal service.

Fortunately, a new breed of high ductility concrete material, generally known as high performance fiber reinforced concrete, or HPFRCC, is being rapidly advanced. The high ductility concrete has orders of magnitude improvement in tensile strain capacity in comparison to normal concrete. While fiber is used in HPFRCC, as in regular FRC, the two materials are significantly different in behavior. Figure 1a shows the high strain capacity of a microstructurally tailored HPFRCC, known as Engineered Cementitious Composite (ECC). In both concrete and FRC, tension softening occurs after a crack is formed in the uniaxial tension specimen. In ECC, the first

cracking point represents the beginning of a damage process. Analogous to ductile metals, ECC shows macroscopic strain-hardening effect, but the inelastic process is one of evolution of multiple microcracks (Figure 1b) instead of dislocation movements in metal after yield. In ECC, the tensile strain capacity can be as much as five hundred times that of normal concrete, before localization into a macroscopic fracture occurs. Thus in most structural applications, it may be expected that fracture failure is suppressed. The development of ECC represents a successful use of micromechanics to provide guidance in systematic material microstructure tailoring to convert a brittle mortar matrix into a ductile concrete material.

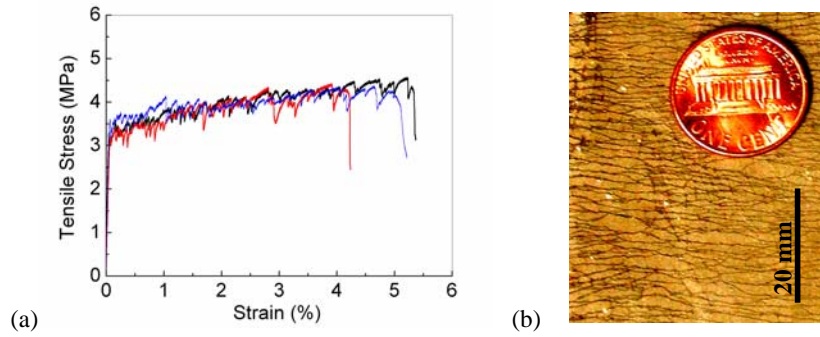(a)   (b)

Figure 1: Tensile behavior of ECC: (a) Stress-strain curve, and (b) Multiple microcracking

This article highlights the fracture phenomena of ECC at the micro and meso-scales, emphasizing the importance of controlling the micromechanical parameters resulting from the description of these fracture phenomena, in order to attain macroscopic ductility. The objective of this article is to make evident the feasibility of material design based on fracture mechanics at the micro and meso-scales, and that fracture failure of composites and structures can therefore be suppressed. In the following, the tunnel cracking responsible for the debonding phenomenon at the fiber/matrix interface and the steady state cracking responsible for the multiple cracking phenomenon of the composite are first described. Material component tailoring is discussed in light of these phenomena. An example of fracture suppression in ECC structural members is reviewed.

2   TUNNELING CRACK AT FIBER/MATRIX INTERFACE

The tunneling crack problem at a fiber/matrix interface with friction (Figure 2) was solved by Lin and Li [1]. Energy balance during tunnel crack advance is given by

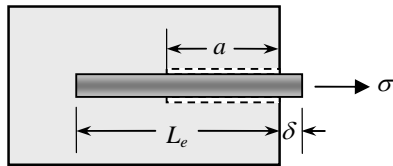$$dW_y = dW_\varepsilon + dW_f + \Gamma_i dA_i \tag{1}$$

Figure 2: Tunneling crack at fiber/matrix interface

where dW_y, dW_e and dW_f are the work done by external forces "applied" to the fiber end (exposed by an imaginary cut of the fiber segment which bridge over a matrix crack), change in strain energy in the fiber and surrounding matrix, and work done by frictional force on the debonded interface, respectively for a given extension da of the debonded interface.

By expressing the energy terms in terms of the elastic deformation behavior of the fiber and the

surrounding matrix material in eqn. (1), the fiber bridging stress σ can be written in terms of the tunnel crack length a and the interface friction τ_0 and debonding fracture energy Γ_i.

$$\sigma = \frac{4\tau_0 a(1+\eta)}{d_f} + \sqrt{\frac{8\Gamma_i E_f(1+\eta)}{d_f}} \tag{2}$$

where E_f and d_f are fiber modulus and diameter, respectively, and η is a parameter expressing the ratio of the effective (accounting for volume fraction) fiber stiffness to effective matrix stiffness. η approaches zero as the fiber content becomes small. The fiber bridging stress versus the pull-out displacement relative to the crack surface u is given by

$$\sigma = 2\sqrt{(\tau_0 u + \Gamma_i)\frac{2E_f(1+\eta)}{d_f}} \tag{3}$$

For debonding of a fiber on both sides of a matrix crack, the crack opening $\delta = 2u$, so that

$$\sigma = 2\sqrt{\left(\tau_0 \frac{\delta}{2} + \Gamma_i\right)\frac{2E_f(1+\eta)}{d_f}} \tag{4}$$

It is interesting to note that the degenerate form of eqn. (2) or eqn. (3) with no interfacial friction (i.e. $\tau_0 = 0$) and with small fiber content ($\eta \longrightarrow 0$), i.e.

$$\sigma = \sqrt{\frac{8\Gamma_i E_f}{d_f}} \tag{5}$$

was first derived by Outwater and Murphy [2]. Without friction, eqn. (5) shows that once the fiber bridging stress reaches the level given by eqn. (5), the tunnel crack will propagate steadily without increase in load, i.e. in steady state. With friction, however, eqn. (2) shows that a linearly increasing load σ is necessary to maintain the continued extension of the tunnel crack a. The maximum fiber stress occurs when the tunnel crack extends to the embedded fiber end:

$$\sigma_0 = \frac{4\tau_0 L_e(1+\eta)}{d_f} + \sqrt{\frac{8\Gamma_i E_f(1+\eta)}{d_f}} \tag{6}$$

where L_e is the embedded fiber length. For random fiber distribution, the maximum value of L_e is half the fiber length L_f. Clearly for a fiber not to break, the maximum stress experienced must not exceed the fiber strength σ_{fu}, i.e.

$$\sigma_0 = \frac{2\tau_0 L_f(1+\eta)}{d_f} + \sqrt{\frac{8\Gamma_i E_f(1+\eta)}{d_f}} < \sigma_{fu} \tag{7}$$

This defines a critical fiber length L_f^c beyond which rupture of fiber may be expected:

$$L_f^c = \frac{d_f\left(\sigma_{fu} - \sqrt{\frac{8\Gamma_i E_f(1+\eta)}{d_f}}\right)}{2\tau_0(1+\eta)} \tag{8}$$

The well known degenerate form of eqn. (8) when chemical bond is absent, i.e. when $\Gamma_i = 0$, and for small fiber content ($\eta \longrightarrow 0$) is

$$L_f^c = \frac{d_f \sigma_{fu}}{2\tau_0} \tag{9}$$

The more complete form of eqn. (8) for critical fiber length emphasizes that fiber rupture can be much more prominent when interfacial chemical bond is present. The second term in the large bracket on the right hand side of eqn. (8) can be considered an effective reduction in fiber strength. A high Γ_i value leads to a larger fiber strength reduction.

The micromechanical parameters within our control are the interface pair (τ_0, Γ_i), and the fiber parameters (d_f, E_f, σ_{fu}, L_f). The most obvious guidance for microstructure tailoring from the consideration that fibers should not break during multiple cracking is that τ_0, Γ_i and L_f must be limited for available fiber strength σ_{fu}. This provides useful information in the optimal treatment (draw ratio, temperature, etc.) of fiber and the type and amount of fiber surface coating. For more detail guidance, it is necessary to review the conditions for multiple cracking, considered next.

3 STEADY STATE PROPAGATION OF BRIDGED MATRIX CRACKS

One of the conditions for multiple cracking is that matrix cracks initiated from defect sites must propagate in a steady state flat crack mode on the meso-scale. (The other condition is that the tensile stress to initiate a matrix crack must be less than the maximum fiber bridging stress). Physically, the flat crack mode (Figure 3) as opposed to the modified Griffith crack mode is necessary because the crack opening cannot increase infinitely even as a matrix crack extends, otherwise fiber breakage or pull-out must occur, thus interrupting the load transfer process from this crack-plane to initiate additional cracks elsewhere.

The condition for steady state cracking for a flat bridged crack was analyzed by Cox and Marhall [3]. Using the J-integral method, they concluded that the matrix toughness J_{tip} must be limited to

$$J_{tip} \le \sigma_o \delta_o - \int_0^\delta \sigma(\delta)d\delta \equiv J_b' \tag{10}$$

Figure 3: Steady state propagation of a flat bridged matrix crack

The right-hand-side of eqn. (10) is the complementary energy J_b' of the bridging springs' σ–δ relation. The σ–δ relation can be derived by summing up the force contributions of fibers at each crack opening δ using the single fiber debonding expression eqn. (4) and the corresponding pull-out behavior after completion of debonding, and by accounting for the randomness of fiber orientation and location relative to a crack plane. Eqn. (11) shows the σ–δ relation for the special case where fibers are aligned normal to a matrix crack and no fiber rupture occurs,
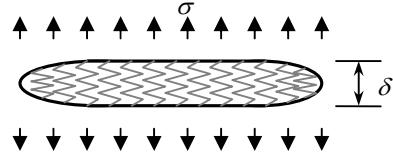
$$\sigma(\delta) = \begin{cases} 2V_f\sqrt{(2\Gamma_i + \tau_0\delta)\dfrac{E_f(1+\eta)}{d_f}} - \dfrac{V_f E_f}{L_f \tau_0(1+\eta)}\left[4\eta\Gamma_i + (1+2\eta)\tau_0\delta - 2\eta\sqrt{2\Gamma_i(2\Gamma_i + \tau_0\delta)}\right] & \delta \le \delta_c \\[2ex] \dfrac{4V_f\tau_0}{L_f d_f}\left(\dfrac{L_f}{2} - \delta\right)^2 & \delta_c < \delta < L_f/2 \end{cases} \tag{11}$$

where δ_c is the crack opening when fibers of all embedment lengths complete debonding.

$$\delta_c = \frac{\tau_0 L_f^2(1+\eta)}{E_f d_f} + \sqrt{\frac{8\Gamma_i L_f^2(1+\eta)}{E_f d_f}} \tag{12}$$

Eqn. (10) provides helpful guidance for tailoring of microstructural parameters. It indicates that there should be an upper limit on matrix toughness, above which steady state cracking cannot occur, and the composite returns to a tension-softening FRC. This upper limit is set by the spring behavior that is in turn governed by the fiber and interface properties as described in eqn. (11). The magnitude of matrix toughness is governed by a number of factors, including the *w/c* ratio, the sand particle size and content, and porosity.

Using eqn. (11) in eqn. (10), the complementary energy can be approximated as

$$J_b' = V_f \frac{L_f}{d_f}\left(\frac{\tau_0^2 L_f^2}{6 d_f E_f} - 2\Gamma_i\right) \tag{13}$$

Eqn. (13) suggests that high fiber aspect ratio L_f/d_f and interface friction τ_0 enhances J_b', and that high chemical bond Γ_i reduces J_b', assuming infinite fiber strength. They are illustrative of the composite design guidelines provided by applying fracture mechanics at the micro and meso-scale in order to attain ductility at the composite scale. Extension of eqn. (11) and eqn. (13) to account for random orientation and rupture of fibers can be found in Li and co-workers ([4], [5]).

4 FRACTURE SUPPRESSION IN STRUCTURAL MEMBERS

ECCs designed according to the micromechanics principles described above have achieved extremely high tensile ductility, as shown in Figure 1. With strain capacity two orders of magnitude higher than that in most concrete materials, the typical fracture failure in concrete structural elements can be fully suppressed.

An example is offered below to illustrate this point. Other examples can be found in investigations on shear connections with steel studs in ECC (Qian [6]), and on precast ECC panels loaded under cyclic shear (Kesner and Billington [7]).

Reinforced ECC columns have been tested (Fischer and Li [8]) under reversed cyclic loading conditions. Figure 4 shows the damage experienced after over twenty cycles of increasing drift up to 10% on a 1/5 scaled element. For comparison, the damage experienced by an R/C element with seismic detailing is also shown. It is clear that the R/ECC was able to withstand large imposed deformation without accompanied by the commonly observed fracture phenomena, including concrete/reinforcement bond splitting, concrete cover spalling, and concrete core crushing. Even without seismic detailing, the ECC material was able to absorb the high shear and flexural forces by undergoing strain-hardening, spreading the damage and engaging a larger portion of the axial steel reinforcement to undergo plastic yielding. As a result, the member becomes more ductile, as shown by the full hysteresis loops in Figure 5a.
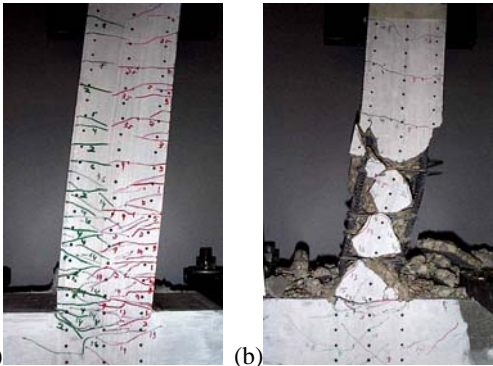

Figure 4: Damage behavior of (a) R/ECC without stirrups, and (b) R/C, shown at 10% drift.
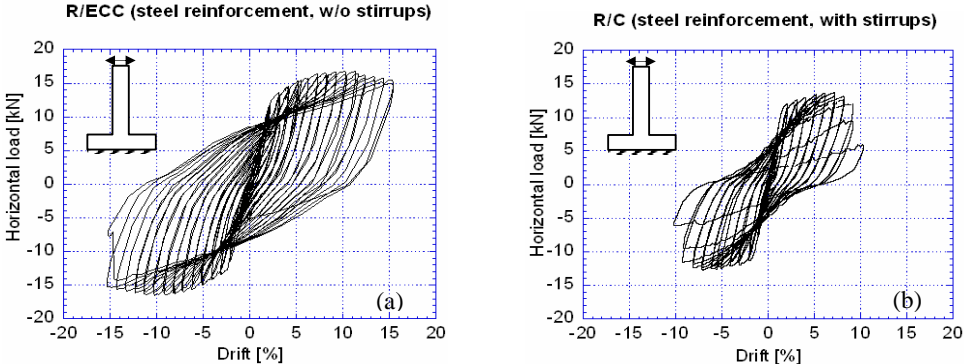

Figure 5: Hysteresis loops of column members under fully reversed cyclic loading for (a) R/ECC without stirrups, and (b) R/C.

The avoidance of bond splitting in R/ECC results from load transfer across the microcracks via bridged fibers in ECC. Thus even as the axial steel reinforcement yields, the ECC deforms compatibility with the steel, and negligible shear force is experienced by the steel/ECC interface. This has been confirmed by measurement of the deformation behavior of R/ECC up to several percent in tension (Figure 6). The suppression of localized fracture is a major contributing factor of ECC in enhancing structural performance.
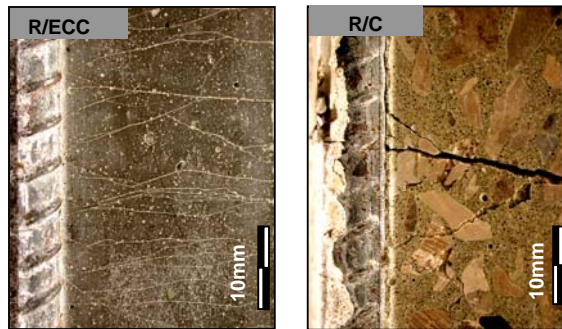

Figure 6: (a) Compatible deformation between ECC and steel, and (b) brittle fracture of concrete in R/C causes high interfacial shear and bond splitting (Fischer and Li [9]).

5 CONCLUSIONS

(1) Macroscopic fracture failure at the structural scale can be suppressed by designing for composite ductility based on fracture phenomena and modeling at the micro and meso scales. The fracture parameters identified includes the fracture energy Γ_i of the fiber/matrix interface, and the matrix toughness J_{tip}. Interestingly, controlled low values of these two fracture parameters are preferred for high composite ductility and suppression of the macroscopic fracture failure mode.
(2) The micromechanics based holistic approach of designing ECC has largely been confirmed by experimental observations on the composite level, and on the structural element levels.

REFERENCES

[1] Lin, Z. & Li, V.C., Crack bridging in fiber reinforced cementitious composites with slip-hardening interfaces, J. Mechanics and Physics of Solids, 45 (5)763-787, 1997.
[2] Outwater, J. D. & Murphy, M.C., On the fracture energy of uni-directional laminates, Proc. of the 24th Annual Technical Conference of the Reinforced Plastics/Composites Division, The Society of the Plastics Industry, Washington, D.C., pp. 11-C-1 - 11-C-8., 1967.
[3] Marshall, D. B. & Cox, B. N., A J-integral method for calculating steady-state matrix cracking stresses in composites, Mechanics of Materials, 8, 127-133, 1988.
[4] Li, V. C., From micromechanics to structural engineering – the design of cementitious composites for civil engineering applications, JSCE J. Struc. Mech. & Earthquake Engineering, 10 (2) 37-48, 1993.
[5] Lin, Z., Kanda, T. & Li, V. C., On interface property characterization and performance of fiber-reinforced cementitious composites, J. Concrete Sci. & Eng., 1, 173-184, 1999.
[6] Qian, S., Kim, Y.Y. & Li, V.C., Influence of concrete material ductility on the behavior of stud shear connection," in Proc. FRAMCOS-5, Colorado, Eds. V.C. Li et al, 1045-1050, 2004.
[7] Kesner, K. & Billington, S. L., Experimental response of precast infill panels made with DFRCC," in Proc. DFRCC Int'l Workshop, Takayama, Japan, pp. 289-298, 2002.
[8] Fischer, G., Fukuyama, H. & Li, V. C., Effect of matrix ductility on the performance of reinforced ECC column members under reversed cyclic loading conditions, in Proc. DFRCC Int'l Workshop, Takayama, Japan, 269-278, 2002.
[9] Fischer, G. & Li, V.C., Influence of matrix ductility on the tension-stiffening behavior of steel reinforced Engineered Cementitious Composites," ACI Struc. J., 99 (1)104-111, 2002.